Flow Modeling of Swagelok's 6L-MPC-WS-SHLG Device

Written by Daniel Yates
Mentored by Professor Bruce Finlayson

University of Washington
Chemical Engineering Undergraduate Research

June 8, 2006

Introduction

This report discusses fluidic modeling research done on the Swagelok 6L-MPC-WS-SHLG component of their Modular Platform Components (MPC) system. The interest came from the University of Washington's Center for Process Analytical Chemistry (CPAC) as part of the New Sampling and Sensor Initiative (NeSSI) that explores systems such as the Swagelok MPC as a means for building lab-on-a-chip type devices.

The MPC system allows small amounts of fluid flow between multiple sensors in series that are chosen based on the experiments needs. Flow between these sensors is possible due to interconnects such as the 6L-MPC-WS-SHLG that is shown in Figure 1. Fluid dynamics of the mixtures in these interconnects have impact on the results obtained from several of the sensors. Exploring the dynamics is difficult to accomplish experimentally in the lab. However, digitally modeling the device and applying dynamic fundamentals can predict the behavior that is occurring. From these results, a full understanding of the results from the sensors can be made. Also, changes to the system can be made to generate dynamics best suited for the application.
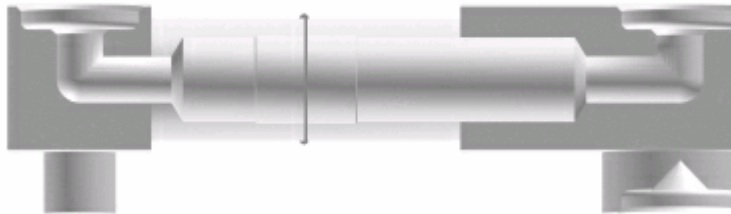

Figure 1. Side-view graphic of the Swagelok 6L-MPC-WS-SHLG interconnect used in their Modular Platform Components (MPC) system. (www.swagelok.com)

Materials and Methods

Modeling and dynamic calculations were performed using COMSOL Multiphysics Suite (COMSOL, Inc.) software. Dimensions of the device partly supplied by employees at Swagelok and partly estimated based on pictures of the device. Appendex A is a PowerPoint slide of the dimensions provided by Swagelok. Those dimensions were converted into metric terms and rounded up for simplified use in COMSOL. Other dimensions were then based on a best guess analysis of a side-view picture of the device pulled from the Swagelok Company website (www.swagelok.com). Figure 2 shows the dimensions, in millimeters, of the model used to generate the results covered in the rest of this paper. The right side was modeled as a mirror of the left. The resulting 3D model is shown in Figure 3, which also shows the model with applied mesh.

3.8 2.4 4.3

5.5 1 18.2

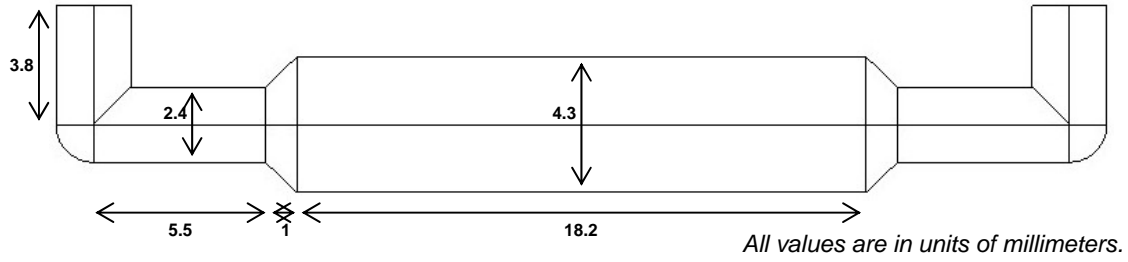All values are in units of millimeters.

Figure 2. Sketch of the Swagelok 6L-MPC-WS-SHLG with dimensions, in millimeters, used to generate a 3D-model for use in dynamic calculations.
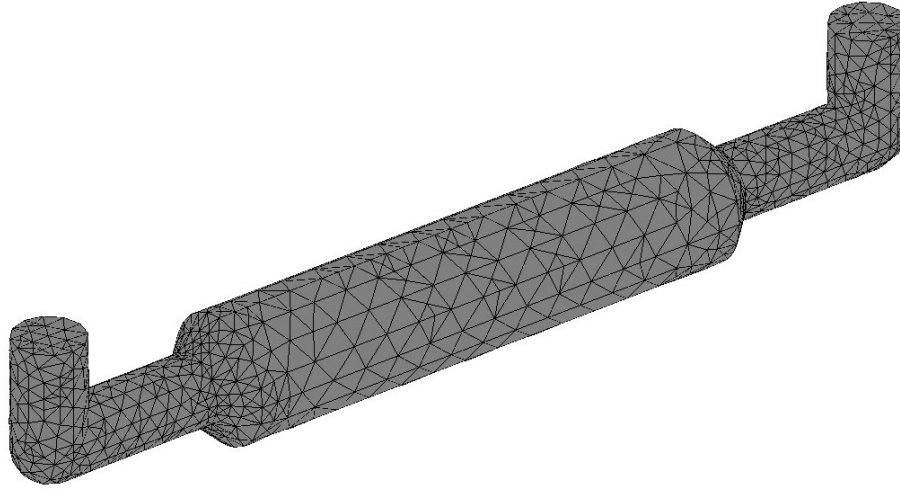

Figure 3. 3D model of the Swagelok 6L-MPC-WS-SHLG with applied mesh. The number of elements was 18846 with 89368 degrees of freedom.

A mesh was applied to the model with 18846 elements and providing 89368 degrees of freedom. To solve for the momentum transport, a stationary nonlinear solver using GMRES chosen to minimize memory consumption, but for convective and diffusive transport the lack of memory was not an issue and so a stationary nonlinear solver using Direct (UMFPACK) was used. The momentum transport was modeled using the Navier-Stokes equation for incompressible fluids, given in Equation 1, and the convective and diffusive transport was modeled using steady-state convection and diffusion equations, given in Equation 2. The momentum transport was solved first and the results obtained were used in solving the convective and diffusive transport.

$$\rho \frac{D\mathbf{v}}{Dt} = -\nabla p + \mu \nabla^2 \mathbf{v} + \rho \mathbf{g}$$

(Eqn. 1)

$$(\nabla \cdot \mathbf{v}) = 0$$

ρ = constant density of fluid

$\mathbf{v}$ = velocity vector

p = pressure

μ = constant dynamic viscosity

$\mathbf{g}$ = gravitational force vector

$$D\nabla^2 c = \mathbf{v} \cdot \nabla c \qquad \text{(Eqn. 2)}$$

D = constant diffusion coefficient
c = concentration
$\mathbf{v}$ = velocity vector

The properties of the fluid were determined to be those similar to water and are provided in Table 1. The diffusion coefficient was desired to be 1.0×10^{-9} m^2/s, but at values much lower than 1.0×10^{-7} m^2/s the solver produced erroneous results.

Table 1. Estimated properties of the fluid to be similar to that of water.

Density, ρ =	1000	(kg/m^3)
Dynamic Viscosity, μ =	1.002×10^{-3}	(Pa·s)
Diffusion Coefficent, D =	1.0×10^{-7}	(m^2/s)

Inlet and outlet boundary conditions were set according to Table 2. The inlet velocity was chosen based on an operating flow rate of 10 mL/min provided by CPAC. Another inlet velocity corresponding to a flow rate of 5 mL/min was examined for momentum transport after looking at the results from the 10 mL/min case. For the convective and diffusive transport analysis, the results from the momentum transport at 10 mL/min flow rate were used. All other boundaries were either 'no slip', for momentum transport, or 'insulated', for convective and diffusive transport.

Table 2. Applied boundary conditions for inlet and outlet boundaries.

	Inlet Boundary Conditions		Outlet Boundary Conditions
	Velocity	**Concentration**	**Velocity/Conc.**
Momentum Tranport	0.036446 m/s or 0.018223 m/s	-	Neutral
Convective and Diffusive Transport	-	Half 1 mM and Half 0 mM	Convective flux

Inlet concentration profile was chosen to show how a difference of concentration at the inlet will change as it progresses through the system. Several variations of the same profile were performed, but they all consisted of a 1 mM concentration on one semi-circle and 0 mM concentration on the opposite semi-circle. The different variations were a result of rotating the dividing line between the two semi-circle concentrations to different positions. The three main variations are shown in Table 3.

To quantify the amount of mixing that occurred from the different variations of the inlet concentration profile, an average variance of the inlet and outlet concentration profiles were calculated according to Equation 3. Furthermore, a percentage of perfect mixing was calculated by dividing the outlet average variance by the inlet average variance and then setting the case of perfectly mixed equal to 100 percent and that of absolutely no change in variance to be 0 percent. The results of these calculations are shown alongside the different orientations in Table 3.

$$var = \frac{\int (c - avg(c))^2 \cdot w}{\int w}$$

$$avg(c) = \frac{\int c \cdot w}{\int w}$$

(Eqn. 3)

var = average variance of concentration

c = concentration

w = velocity component normal to the outlet boundary

Results

The results can be divided into two sections; momentum transport and convective and diffusive transport.

Momentum Transport

An x-slice and y-slice plot of the momentum transport model can be shown in Figure 4 and Figure 5, respectively, for the velocity field at a 10 mL/min flow rate. The x-axis is in the direction of the length of the device, the y-axis is in the direction of the width or depth of the device, and the z-axis is in the direction of the height of the device. Inlet velocity was set at the boundary in the bottom left of each figure.
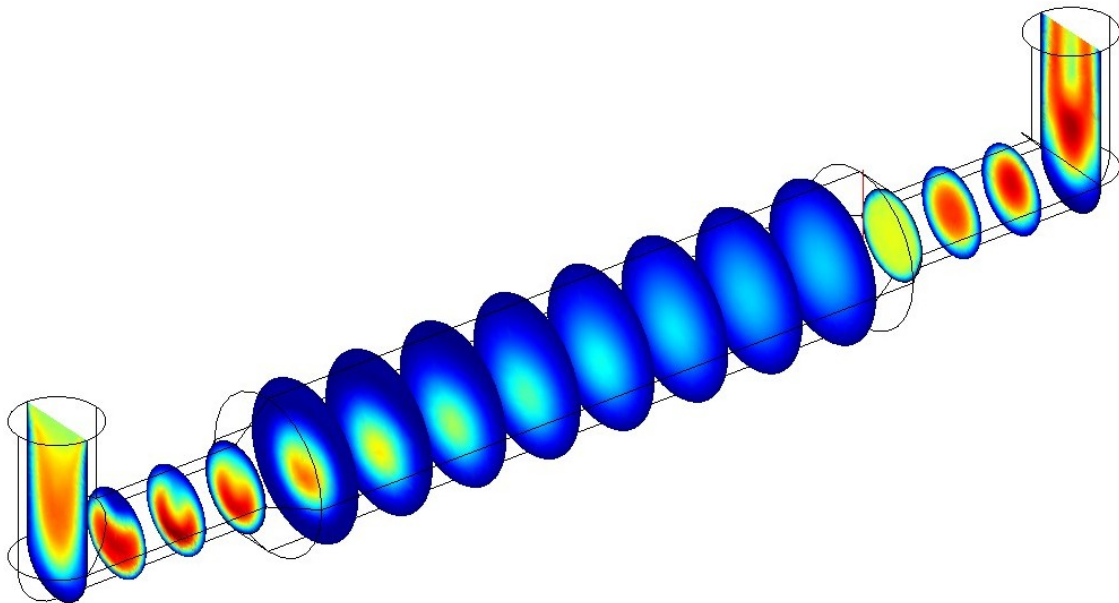

Figure 4. X-slice plot of the velocity field with inlet velocity set at the bottom left of the device.
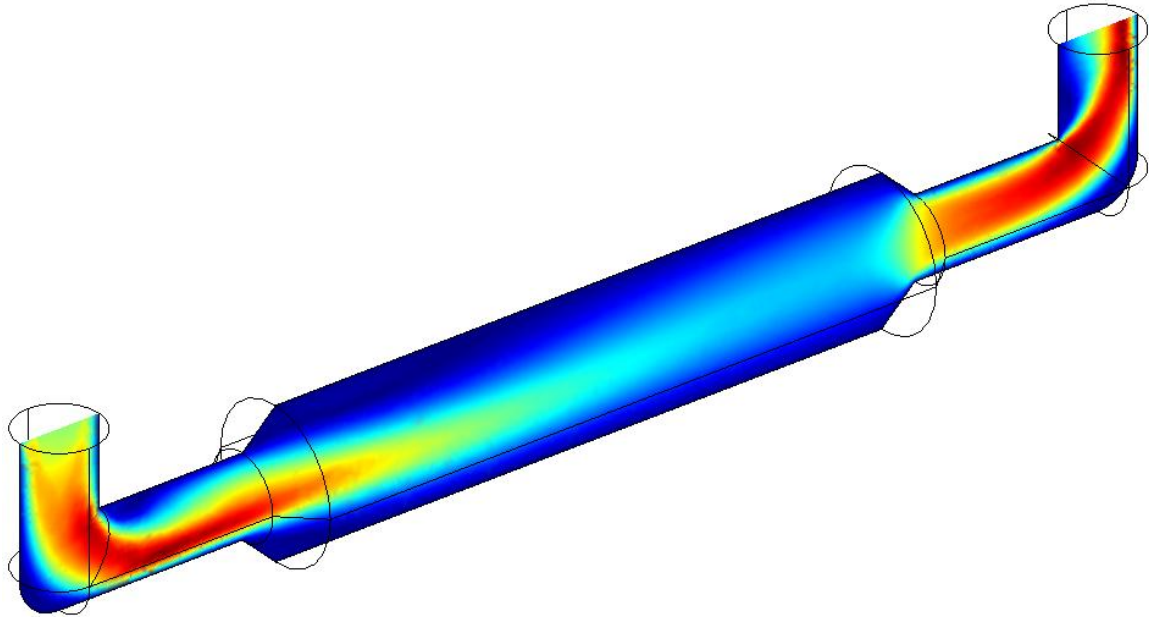
Figure 5. Y-slice plot of the velocity field with inlet velocity set at the bottom left of the device.

To compare the difference of flow rate on flow through the device, a stream line analysis with 22 starting points was made for both the 10 mL/min and 5 mL/min cases. Figure 6 was the results from a flow rate of 10 mL/min and Figure 7 from a flow rate of 5 mL/min. Figure 6 is a streamline plot of the velocity field in a side view, xz-plane, of the model. It was produced using 22 starting points.
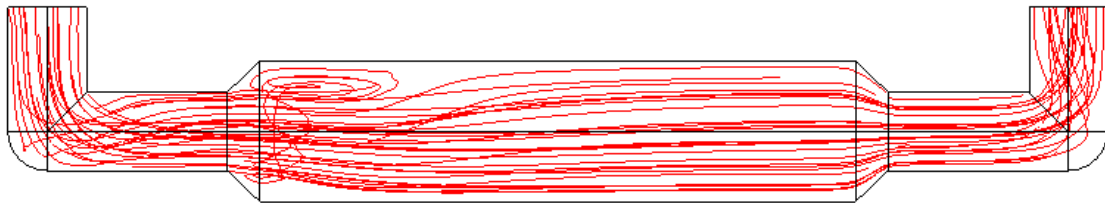

Figure 6. Streamline plot of the velocity field in the xz-plane of the model with a flow rate of 10 mL/min.
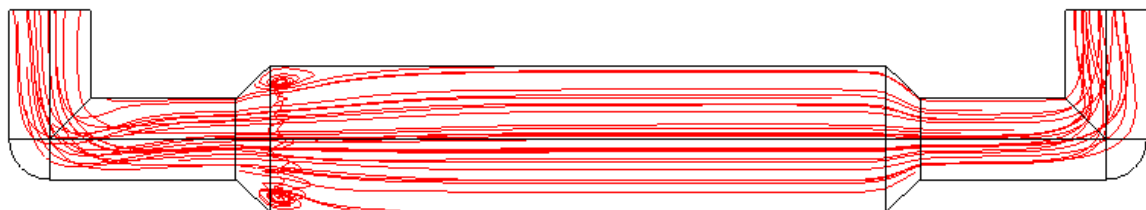

Figure 7. Streamline plot of the velocity field in the xz-plane of the model with a flow rate of 5 mL/min.

Calculation of the Reynolds number for the 10 and 5 mL/min cases were determined to check the validity of the results found. Using the same properties as those in Table 1, the

Reynolds numbers were calculated at the inlet to the device and the results are given in Table 3.
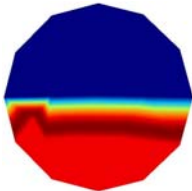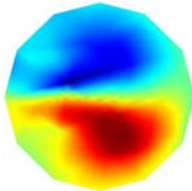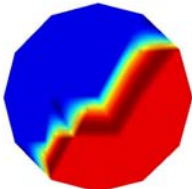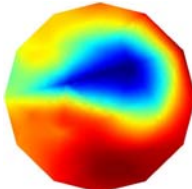
Table 3. Reynolds numbers determined for a flow rate of 10 and 5 mL/min at the inlet to the device.

Inlet Diameter (in)	Flow Rate (mL/min)	Avg. Velocity (in/s)	Reynolds #
0.095	10	1.43	88
0.095	5	0.72	44

Convective and Diffusive Transport

As mentioned in the Materials and Methods, different inlet concentration profiles were modeled and the resulting outlet concentration profiles were examined. The difference between them was only that of orientation, which was changed in a manner that would produce different concentration flow patterns. The results are given in Table 4. Multiple variations of profiles 2 and 3 were considered for difference of location of the more concentrated region relative to the model, but they produced results with differences within the error of the calculations. This included all four variations of the diagonal profile, two with a negative slope dividing and two with a positive slope dividing, and two variations of the number 3 vertical dividing profile, 1 mM concentration on the left and then on the right.

Table 4. Different variations of inlet concentration profiles, their resulting outlet average variance, and percent of complete mixing (red = 1 mM, blue = 0 mM).

	Inlet Conc.	Outlet Conc.	Outlet Average Variance	Percent Perfectly Mixed
1			0.076	68.2%
2			0.045	81.0%

3		0.034	85.6%
4		0.00	100.0%
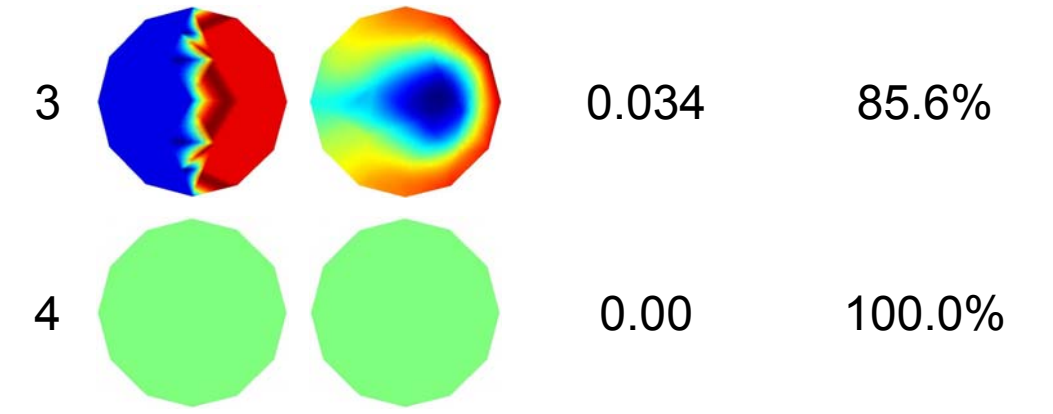
As was done with the Reynolds number for the momentum transport, the Peclet number was calculated at the inlet to provide a check of the observed results. For a flow rate of 10 mL/min, an inlet diameter of 0.095 in., and fluid properties as listed in Table 1, the Peclet number was calculated to be 879.

Discussion

Momentum Transport

Determination of the velocity field through the device provided some interesting results. From Figures 4 and 5, it is seen that majority of the fluid will travel at higher velocities on the bottom of the device because of the sharp turn. This does not allow the fluid to recover to fully developed flow before the expansion and thus contributes to the formation of a vortex, as seen in Figure 6. However, the sharp turn was not the only thing to contribute to the formation of a vortex. Even at a flow rate of 5 mL/min, as seen in Figure 7, the vortexes are still present. The slope of the transition to the expansion chamber was much steeper than the flow rate would allow for a smooth transition. Thus, the removal of the vortexes would require running at a lower flow rate or designing the device to have a shallower slope on the transition in.

At the other end of the device, in the contraction back to the smaller diameter pipe, it was observed from Figures 4 and 5 that the velocity field nears that of fully developed flow. Also, the problems associated with the steepness of the transition into the larger diameter pipe are not a problem on the contraction to the smaller diameter pipe, regardless of flow rate.

Comparison of the modeling results and the dimensionless number analysis agree. The fluid at the inlet has a Reynolds number in the laminar regime and the results obtained from modeling show patterns of laminar flow.

Convective and Diffusive Transport

From examining the results shown in Table 4, it seems that there should be quite a bit of mixing occurring in the device. Based on the results of calculating the Peclet number, the

mixing was most influenced by mechanical means, such as the sharp elbow turns, and less influenced by diffusive means. If such was the case, than decreasing the diffusion coefficient to its intended value of 1 x 10^{-9} m/s^2 would have little impact on the amount of mixing that occurs, as quantified by the average variance values of the outlet concentration profile.

In analyzing different inlet concentration profiles and calculating the average variances, it was found that the least mixing occurred when the profile was symmetric with the rest of the model, number 1 in Table 4, and the most mixing occurred when the profile was asymmetric with the model, number 3 in Table 4. This can be seen in their respective outlet profiles where in the least mixed case the inlet and outlet profiles are nearly alike, but in the most mixed case the outlet profile takes on a new form from mechanical mixing that is occurring in the device. Also, results from the diagonal inlet profile, number 2 in Table 4, was closer to that of the asymmetric profile, number 3 in Table 4, than to the symmetric profile, number 1 in Table 4. It could be estimated that the change in average variance at the outlet decreases more sharply as the inlet profile just starts differing from the symmetric profile.

Conclusion

The design of the device to provide flow from one module to another appears to have some unexpected results. Formation of vortices, even at lower flow rates, may cause problems that would affect experimental results from module sensors attached to the system. It was also found that mixing occurs largely due to non-diffusive effects. The inlet and associated outlet profiles will provide for a better understanding of the device and the design or use of sensor modules for more accurate results.
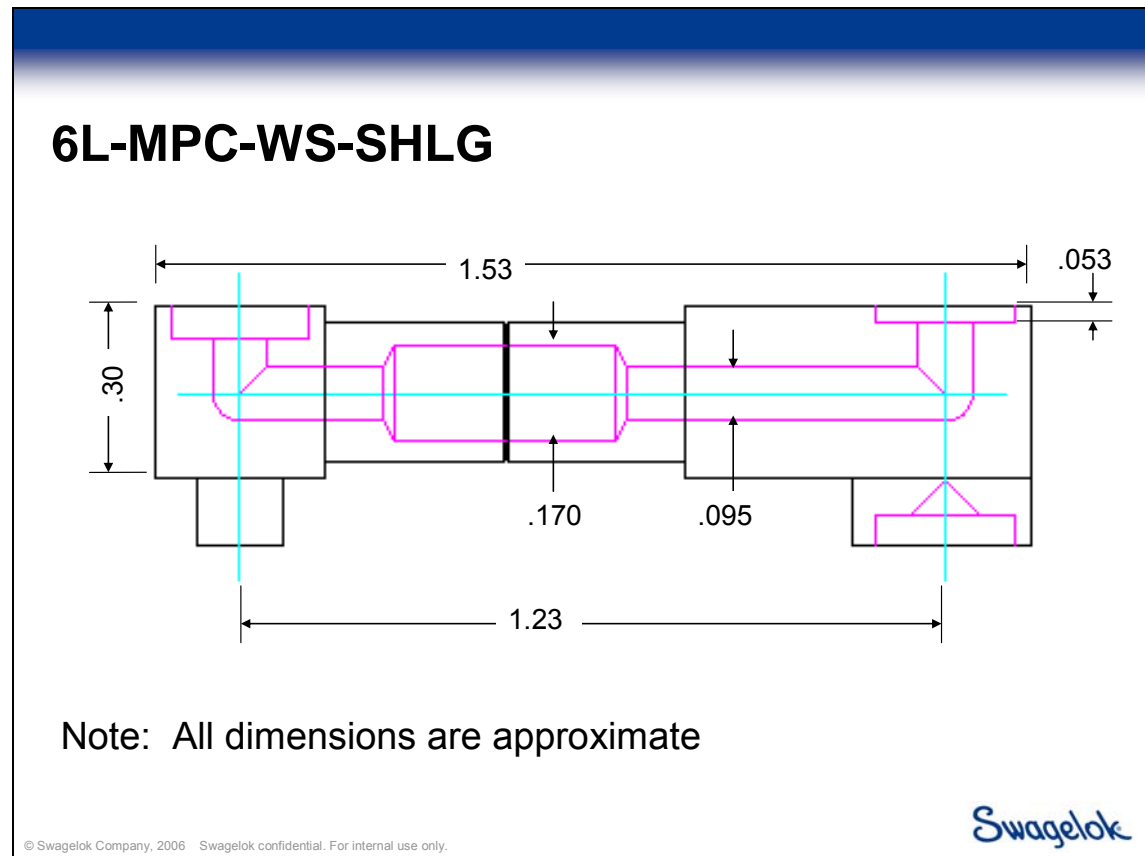
Appendix A

Figure A1. Dimensions, in inches, of the 6L-MPC-WS-SHLG device that was provided by employees of Swagelok for use in modeling.